3D Numerical Study and Parametric Analysis of PV/T Design Effect on Thermal and Electrical Performance

Ahmed Saad Eddine Souissi

Industrial Engineering Department, College of Engineering, Northern Border University, Saudi Arabia
souissi.ahmed@gmail.com

Majed Masmali

Industrial Engineering Department, College of Engineering, Northern Border University, Saudi Arabia
majed.masmali@nbu.edu.sa

Mohamed Fterich

Industrial Engineering Department, College of Engineering, Northern Border University, Saudi Arabia | Laboratory of Electromechanical Systems (LASEM), University of Sfax, 3038 Sfax, Tunisia | mohamed.fterich@enis.tn (corresponding author)

Ezzeddine Touti

Department of Electrical Engineering, College of Engineering, Northern Border University, Arar, Saudi Arabia | Department of Electrical Engineering, Higher Institute of Applied Sciences and Technology of Kasserine, Kairouan University, Kairouan, Tunisia
ezzeddinetouti@gmail.com

Houssam Chouikhi

Laboratory of Electromechanical Systems (LASEM), University of Sfax, 3038 Sfax, Tunisia | Mechanical Engineering Department, College of Engineering (CoE), King Faisal University (KFU), PO Box 380 Al-Ahsa 31982, Kingdom of Saudi Arabia
h.chouikhi@gmail.com

ABSTRACT

This paper explores the influence of design variations on the electrical and thermal efficiencies of PV/T (Photovoltaic-Thermal) systems. Utilizing COMSOL Multiphysics, three different PVT configurations with varying air duct designs were studied. The results demonstrated significant enhancements in both electrical and thermal efficiencies, with the PVT-3 configuration outperforming PVT-1 and PVT-2. Specifically, PVT-3, incorporating fin-shaped air ducts, exhibited the lowest recorded panel temperature of 55 °C, indicating improved electrical efficiency and thermal performance. Also, PVT-3 achieved the highest average thermal efficiency of 46.35% and the best electrical performance of 13.91%. Furthermore, the study highlights ameliorated airflow dynamics and uniformity within the ducts, particularly with the redesigned air inlet. These findings underscore the importance of design innovations in optimizing temperature management and energy output in PVT systems. It is worth noting that the tests were conducted under identical operating conditions, including air velocity, inlet temperature, ambient temperature, and solar irradiation.

Keywords-PV/T air collector; air ducts; 3D numerical simulation; Comsol Multiphysics; heat transfer; electrical characteristics

I. INTRODUCTION

Solar energy stands out as the most promising among renewable resources, offering an endless and exceptionally reliable technology for clean energy [1]. This energy undergoes conversion into thermal and electrical forms [2], prompting the development of an optimized solar collector known as the hybrid Photovoltaic-Thermal (PV/T) collector [3]. However, its efficiency often decreases with the rise in the module's temperature [4], and the extent of power loss is contingent on the specific configuration of each PV/T design. The improvement of solar energy utilization is a primary research objective [5]. Hence, implementing cooling mechanisms to absorb heat from PV modules is essential for enhancing electrical efficiency [6]. Furthermore, the reclaimed heat can be utilized in various applications, such as drying processes [7]. Hybrid PV/Ts aim to upgrade the electrical efficiency of PV panels by absorbing the heat stored in the PV cells [8]. Nevertheless, thermal effectiveness depends on solar intensity and mass flow rate, with electrical performance enhanced as cell temperature decreases due to the corresponding increase in the mass flow rate [9]. Numerous configurations have been adopted to improve efficiency. Studies [10-11] on hybrid PV/T solar collectors showed a direct correlation between panel temperature and electrical energy production, with thermal energy production exceeding three times the output of electrical energy. Incremental modifications in PV/T component design were investigated for efficiency enhancements, revealing a functional interdependence between working fluid and collector design [12]. Authors in [13] examined the electrical performance of a PV/T system using a flowing nanofluid and nano-paraffin wax for cooling, achieving a maximum efficiency of 13.7%, a significant improvement over the conventional PV system's 7.1% efficiency. The flow rate notably influenced thermal efficacy, determined by the convective heat transfer impacted by the flow velocity [14-15]. While the production cost of a PV/T system is economically viable, ensuring a stable electrical output necessitates effective cooling of the PV cell [16]. Elevated temperatures negatively impact PV panel performance, emphasizing the need for enhanced cooling methods in PV/T technology development. Future endeavors should prioritize improvements in PV cell cooling to maintain a consistently low and stable operating temperature [17]. Employing wasted heat energy from the PV panel in the drying system generated greater output voltage from the harvesting system [18-19]. A research effort focused on synergistically integrating a PV panel with a Thermoelectric Generator (TEG) to optimize the energy yield and enhance the overall system efficiency was conducted in [20]. This strategy, harnessing waste heat loss from the PV cell, substantially ameliorated the overall performance of the PV panel system.

Despite the numerous efforts in various studies, the need for the development of new prototypes and a more comprehensive heat transfer analysis remains. The objective of this work is to enhance heat dissipation within a PV/T device to mitigate cell heating. The current study investigates the thermal dynamics of developed PV/T prototypes, examining heating and cooling behaviors, and tracking the temperature progression of airflow within air channels. The authenticity of this study allows for a nuanced exploration of the impact of air

duct engineering, identifying optimal designs to ensure a balanced and uniform airflow distribution. This facilitates efficient cooling of the PV panel by effectively absorbing the maximum stored heat within the solar panel. Furthermore, the performed simulation quantifies heat transfer magnitude, assesses the cooling effect of airflow through the air ducts, and predicts the air temperature at the outlet. Therefore, the contribution of this study lies in the thorough evaluation and analysis of the geometric design's impact on the electrical and thermal performances of the hybrid PV/T solar air collector.

II. MATERIALS AND METHODS

A. PV/T Design

The schematic representation of the (PVT) air collector is illustrated in Figure 1, featuring six integral components: (1) air ducts, (2) PV panel, (3) glass layer, (4) insulation layer, and (5) aluminum sheet. An 8 (mm)-thick glass layer is strategically installed above the collector's surface to mitigate the heat loss and optimize the heat transfer. Below the glass, a 5 mm thick PV panel is positioned, maintaining a 20 mm gap to facilitate airflow circulation across the panel's surface. Longitudinally spaced and parallel air ducts at 40 mm intervals separate the contact surface between the PV panel and the aluminum sheet. To prevent air leakage, a 15 mm thick aluminum plate is positioned beneath the air ducts. Furthermore, an insulation layer comprising 5 cm glass wool is applied at the PVT's bottom and sides to effectively minimize the heat energy losses. For a comprehensive overview of the PVT air collector's design and specifications employed in the experimental test, see Table I.
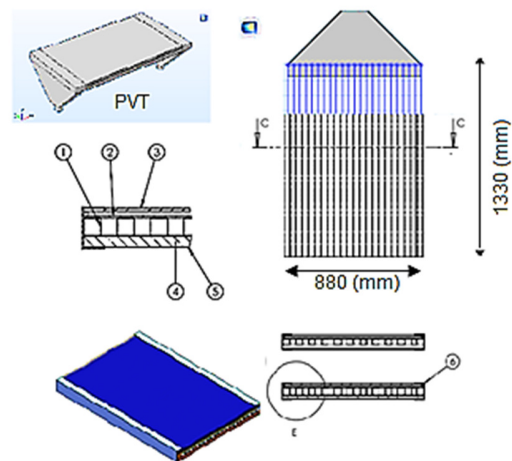

Fig. 1.   Schematic view of the PVT design: (1) Air duct, (2) PV panel, (3) glass, (4) insulation, (5) aluminum sheet, and (6) air gap.

TABLE I.   SPECIFICATIONS OF THE TESTED PV/T MODULE

Material	Polycrystalline silicon
Size	1.33m × 0.88 m × 0.005 m
Area (m²)	1.145
P_{max} **(W)**	165
V_{OC} **(V)**	25
I_{SC} **(A)**	8.61
V_{mpp} **(V)**	20.61
I_{mpp} **(A)**	8.1

B. Numerical Simulation

In order to investigate the performance of the PV/T module with the new air duct designs, temporal numerical simulations were conducted using the finite element software COMSOL Multiphysics. In the numerical simulations aimed at assessing the performance of the PV/T module with the new air duct designs, several foundational assumptions were established. Firstly, the cooling channels were assumed to exhibit perfect homogeneity and incompressibility in the flow. Additionally, thermal-physical properties remained constant despite temperature fluctuations, and the laminar flow was presumed within the air ducts. Moreover, an equilibrium thermodynamic state was assumed between the fluid and solid phases, with the sky modeled as a black body emitting long-wavelength radiation at an equivalent temperature. It was also assumed that the PV/T collector was free from any air leaks, and viscous dissipation was treated as minimal. Lastly, no significant thermal balance was assumed between the fluid and solid phases. These assumptions form the basis for the numerical simulations, enabling a comprehensive analysis of the PVT module's performance across diverse scenarios.

Equation (1) presents the primary partial differential equations governing the thermal energy within the solid layers of the PV/T system, while equation system (2) encompasses the continuity and momentum equations for the fluid layer.

$$\frac{\partial u}{\partial x} + \frac{\partial v}{\partial y} + \frac{\partial w}{\partial z} = 0 \tag{1}$$

$$\begin{cases} u\frac{\partial u}{\partial x} + v\frac{\partial u}{\partial y} + w\frac{\partial u}{\partial z} = \vartheta\frac{\partial^2 u}{\partial x^2} - \frac{1}{p}\frac{\partial p}{\partial x} \\ u\frac{\partial v}{\partial x} + v\frac{\partial v}{\partial y} + w\frac{\partial v}{\partial z} = \vartheta\frac{\partial^2 v}{\partial y^2} - \frac{1}{p}\frac{\partial p}{\partial y} \\ u\frac{\partial w}{\partial x} + v\frac{\partial w}{\partial y} + w\frac{\partial w}{\partial z} = \vartheta\frac{\partial^2 w}{\partial z^2} + \rho.g \end{cases} \tag{2}$$

Considering that heat transfer principles are pivotal in the proposed model for analyzing temperature distribution, this study has formulated the set of equations (3) to elucidate the heat transfer mechanisms within the diverse layers of the PV/T system.

$$\begin{cases} \rho.Cp\frac{\partial T}{\partial t} + \rho.Cp.u\frac{\partial T}{\partial x} - \lambda\frac{\partial^2 T}{\partial x^2} = 0 \\ \rho.Cp\frac{\partial T}{\partial t} + \rho.Cp.u\frac{\partial T}{\partial y} - \lambda\frac{\partial^2 T}{\partial y^2} = 0 \\ \rho.Cp\frac{\partial T}{\partial t} + \rho.Cp.u\frac{\partial T}{\partial z} - \lambda\frac{\partial^2 T}{\partial z^2} = 0 \end{cases} \tag{3}$$

To investigate the electrical characteristics of the PV module within the proposed PV/T designs, a simplified approach is adopted for the sake of clarity. Specifically, a single-diode model is employed. By applying Kirchhoff's current law to this model, a comprehensive equation that captures the voltage-current (V-I) characteristics of the system is derived:

$$I_{pv} = I_{ph} - I_s.[\exp(\frac{q.(V_{pv} + R_s.I_{pv})}{A.K.T_{wo}}) - 1]$$
$$- \frac{(V_{pv} + R_s.I_{pv})}{R_{sh}} \tag{4}$$

1) Boundary Conditions

The quantity of the energy absorbed by the PV/T from the sun is described by:

$$Q_{abs} = \alpha_g.\tau_g.Ird.A_{PVT} \tag{5}$$

The rate of heat loss by natural convection at the top and bottom of the PV/T collector is computed by:

$$Q_{cv} = h_w.A_g.\left(T_g - T_a\right) \tag{6}$$

The heat convection coefficient (h_w) is given by:

$$h_w = 2.8 + 3 \times w_s \tag{7}$$

The radiation losses are calculated as follows:

$$Q_{rd} = \varepsilon_g \times \sigma \times A_g \times \left(T_g^{\,4} - T_a^{\,4}\right) \tag{8}$$

Solid-liquid walls without viscous stress are subject to non-slip conditions. They are described by:

$$\begin{cases} u = 0 \\ v = 0 \\ w = 0 \end{cases} \tag{9}$$

Thermal insulation is described by:

$$-n\left(-K\ \nabla\ T\ \right) = 0 \tag{10}$$

The boundary conditions in the back side of the glass layer are described by:

$$\begin{cases} -\lambda_g\frac{\partial T}{\partial z} = hc_{g-D1} \times \left(T_g - T_{D1}\right) \\ For\ x = 0, \frac{\partial T}{\partial x} = 0 \end{cases} \tag{11}$$

The upper surface boundary conditions of a PV panel are described by:

$$\begin{cases} -\lambda_{pv}\frac{\partial T}{\partial z} = hc_{pv-D1} \times \left(T_{pv} - T_{D1}\right) \\ For\ x = l, \frac{\partial T}{\partial x} = 0 \end{cases} \tag{12}$$

Equation system (13) defines the boundary conditions of the PV panel's back surface:

$$\begin{cases} -\lambda_{pv}\frac{\partial T}{\partial z} = hc_{pv-D2} \times \left(T_{pv} - T_{D2}\right) \\ For\ x = 0, \frac{\partial T}{\partial x} = 0 \end{cases} \tag{13}$$

The rear side of the PV/T collector is described by the following conditions:

$$\begin{cases} T = T_a \\ x = l, \\ \dfrac{\partial T}{\partial x} = 0 \end{cases} \qquad (14)$$

The limit conditions at the outlet of the PV/T are defined by:

$$P = P_{atm} \qquad (15)$$

2) Cross Section of the developed PV/T Designs

To study the intricate relationship between air duct design and its direct impact on both the PV temperature and the outlet temperature, as well as to address the resulting effects on the overall efficiency and the lifespan of the PV system, three PV/T systems with different air duct configurations were tested. Figure 3 portrays the main size of the PV/T prototype and the cross-section views of the three designs of the PVT air collector. The air ducts in all of the designs are arranged longitudinally and in parallel to avoid high-pressure drops. From the inlet, cooling air flows through the gap on the top surface and the air ducts on the bottom surface of the PV panel.
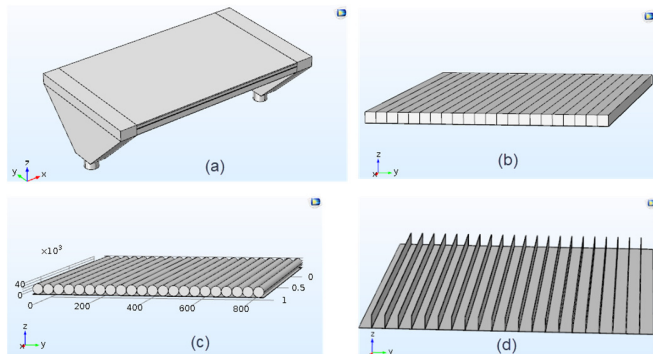
Fig. 2.   Main shape and cross-section view of the proposed PV/T designs: (a) Main shape of the PVT, (b) PVT-1 with square tubes, (c) PVT-2 with tube circle, and (d) PVT-3 with fin-shaped air ducts.

PVT-1 features square tube air ducts measuring 40 mm × 40 mm, while PVT-2 utilizes circular tubes with a diameter of 40 mm. PVT-3, on the other hand, employs fin-shaped air ducts with a width of 40 mm. To assess the significance of selecting the air inlet location for the PV/T unit and examine the impact of this point on the air distribution within the air ducts, two cases of the same PV/T unit were studied, differing only in the air inlet location. Figure 3 presents the two proposed systems with different positions of the air inlet.

3) Meshing of the Photovoltaic Thermal Collector

The thermal and fluid dynamics characteristics were examined through Computational Fluid Dynamics (CFD) simulations conducted using the COMSOL Multiphysics software.
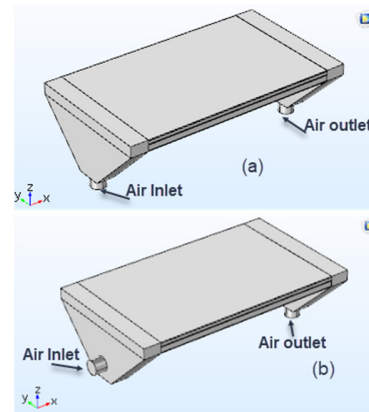
Fig. 3.   PVT designs with two air inlet scenarios: (a) PVT with Inlet-1, (b) PVT with Inlet-2.

Figure 4 displays a simplified mesh model crafted for the analytical study. To assess the model's applicability and alignment with the designed prototype, three governing equations, namely the energy equation, radiation equation, and k-ε equation, were deployed. The Reynolds-Averaged Navier-Stokes (RANS) method is chosen to minimize computational expenses, involving averaging of velocity and pressure fields over time. The equation system is formulated within COMSOL Multiphysics, where heat transfer and airflow distribution are interlinked through non-isothermal flow Multiphysics.
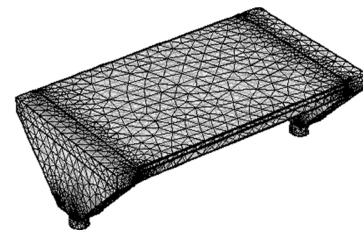
Fig. 4.   Finite element meshing of the PV/T collector.

For conducting the numerical simulation, it is essential to input the physical characteristics of the materials comprising the PV/T layers. Table II provides an overview of the physical properties of the PV/T layers used in the ongoing simulation.

TABLE II.   TABLE 2: THERMOPHYSICAL PROPERTIES AND GEOMETRIC DIMENSIONS OF THE EXPERIMENTAL PVT

Parameter	Value	Parameter	Value
ρ_g	2200 kg/m³	δ_{pv}	0.05 m
ρ_{pv}	2329 kg/m³	δ_{al}	0.005 m
ρ_{al}	2700 kg/m³	$\sigma\,(\frac{W}{m^2 K^4})$	5.670373.E-8
λ_g	1.8 W/m.K	ε_g	0.88
λ_{pv}	130 W/m.K	α_g	0.066
λ_{al}	238 W/m.K	τ_g	0.95
Cp_g	720 J/kgK	ε_{pv}	0.95
Cp_{al}	900 J/kgK	α_{pv}	0.85
Cp_{pv}	700 J/kgK	τ_{pv}	0.87
δ_g	0.08 m		

III.   RESULTS AND DISCUSSION

The operational conditions implemented in the simulation, such as solar radiation, ambient temperature, and inlet temperature of the PV/T are exhibited in Figure 5. Solar radiation varied between 373 W/m² and 780 W/m². Ambient temperature varied between 21.53 °C and 25.83 °C. The inlet temperature varied between 27.18 °C and 34.87 °C.
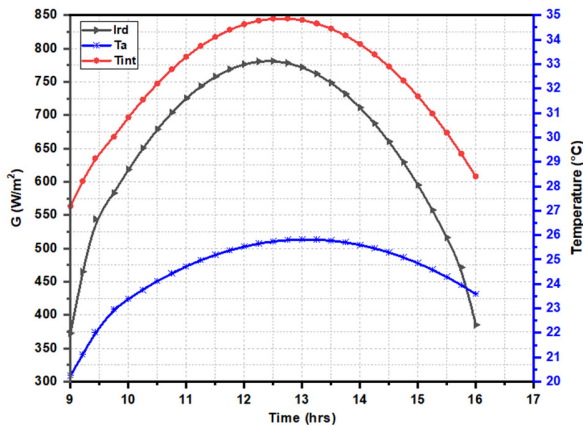

Fig. 5.   Operational conditions.

A. Effect of Air Duct Designs on PV and Outlet Temperatures

The design of the PV/T plays a crucial role in cooling the PV panel through the air ducts located beneath. A numerical examination of the three considered PV/T designs was realized using COMSOL Multiphysics. According to the results depicted in Figure 6, the temperature of the PV panel decreased from one design to another as the configuration of the air ducts changed. Thus, the temperature of the PV module decreased from 61.5 °C with the square-shaped air duct (PVT-1) to 57 °C with the cylindrical-shaped air duct (PVT-2). Subsequently, the temperature decreased further to 55 °C with the featuring fin-shaped air ducts (PVT-3).
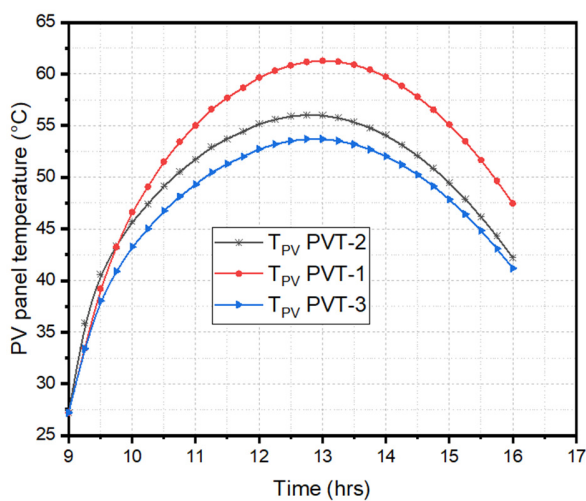

Fig. 6.   PV panel temperature progression according to the air duct geometry.

A larger contact area of the air with the panel's surface enhances the efficiency of cooling the PV cells. In the comprehensive exploration, this study delved into the intricate relationship between the outlet temperature and the varying designs of the air ducts. The discerned patterns in the obtained results unequivocally illustrate a direct correlation: as the contact area of the air with the panel's surface expands, there is a corresponding rise in the outlet temperature (See Figure 7). Also, the simulation results indicate that the cooling of the PV panel resulted in a temperature decrease at the outlet to 59.5 °C in the second design (PVT-2) compared to 57 °C within the first design (PVT-1). Furthermore, the temperature continued to decrease, reaching 55 °C in the third design (PVT-3).
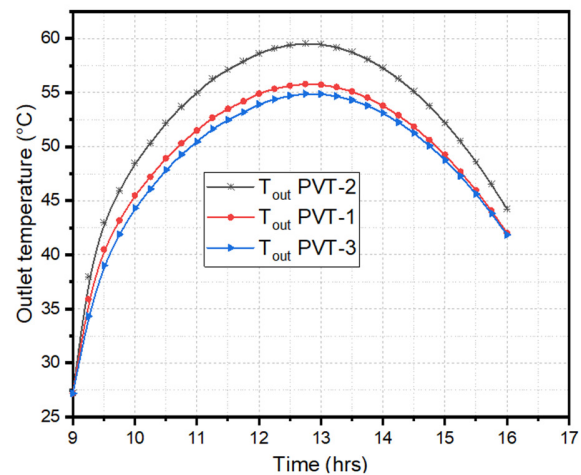

Fig. 7.   Outlet temperature change according to the air duct geometry.

B. 3D Distribution of the Air Flow and Temperature of the Proposed PV/T Designs

A comprehensive 3D analysis of the air distribution within the air ducts was conducted for the three proposed PVT configurations. The simulation results, as depicted in Figure 8, reveal a progressive enhancement in aerodynamic distribution from one design to the next. Notably, the outcomes indicate that the design featuring thin fin-type air ducts (PVT-3) excels in achieving superior air uniformity within both the ducts and gaps. Additionally, a 3D study was carried out on the temperature distribution of the photovoltaic panel for all the proposed PV/T designs. The findings depicted in Figure 9 reveal noteworthy insights into the cooling efficiency of the PV panel across the examined collector models. Among these designs, the third design demonstrated the most effective cooling performance. Specifically, the temperature of the solar panel exhibited a gradual decrease, transitioning from 60°C with PVT-1 to 59°C with PVT-2, and finally reaching 57°C with PVT-3. This observed temperature reduction signifies the superior thermal regulation capabilities of the third collector model, showcasing its ability to maintain a lower operating temperature for the PV panel. These nuanced temperature variations underscore the significance of the design features and characteristics unique to PVT-3, making it a standout choice for optimizing the cooling performance of the solar panel within the studied context.
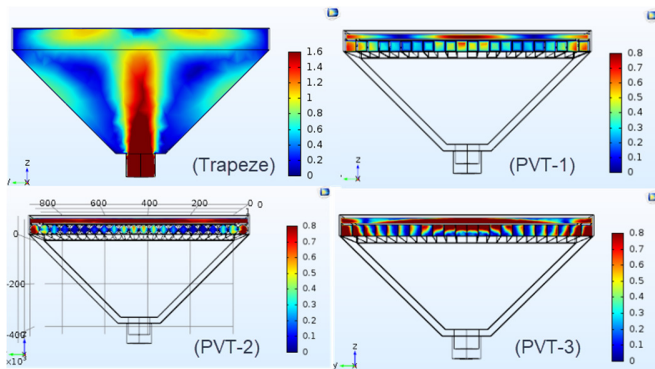
Fig. 8.   3D air flow distribution through the air duct of the proposed designs.
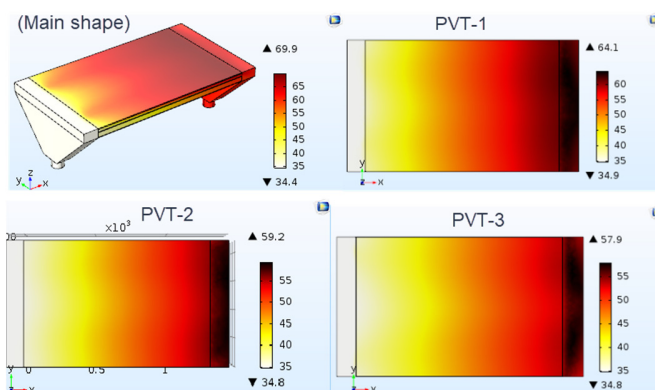

Fig. 9.   3D temperature distribution in the main shape of the PV/T and the PV panel for the three studied designs.

C. Electrical Characteristics of the Proposed PV/T Designs

In Figure 10, the I-V and P-V characteristics evaluation for the developed PV/T systems is presented, showcasing their dependence on the operating temperature of the PV cell. Notably, the short-circuit current exhibited an increase with rising temperature, resulting in a comparatively milder reduction in the open-circuit voltage and a decrease in power as the temperature rose. The primary objective of the current study is to evaluate the impact of the air duct design on critical performance parameters, specifically the delivered power and the produced voltage at the PV/T outputs.

The maximum power values delivered by the PV/T collector for the tested designs, i.e. PVT-1, PVT-2, and PVT-3 were 82 W, 95 W, and 120 W, respectively. The results resoundingly affirm the superior electrical performance of PVT-3, offering compelling evidence that the strategic augmentation of the contact area between air and the PV panel significantly amplifies the overall electrical output of the PV/T system. This noteworthy improvement can be directly attributed to the profound impact of the air channel design on PV/T temperature, orchestrated through the cooling phenomenon. These findings provide valuable insights into the nuanced optimization of the air duct design, paving the way for enhanced electrical performance in PV/T systems.
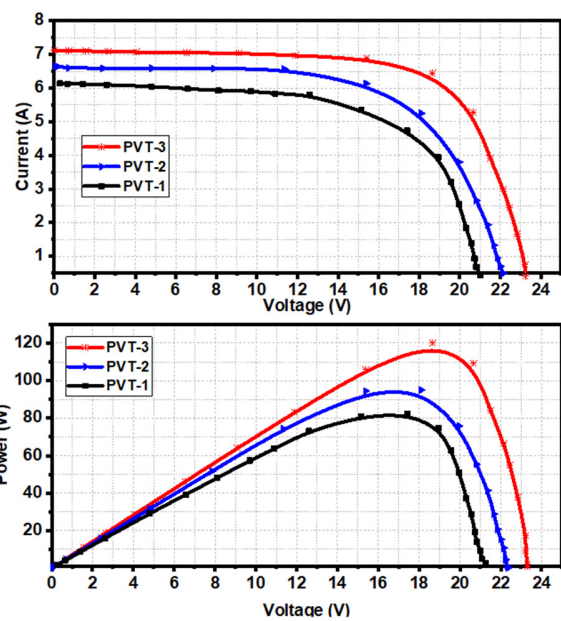

Fig. 10.   Electrical and thermal performance progression of the proposed PV/T designs.

D. Influence of Air Inlet Location on the Cooling Efficiency of Photovoltaic Panels

From the numerical results, a non-uniform air distribution in all the examined PV/T designs was noted, specifically in the trapezoidal section located at the beginning of the PV/T setup. This non-uniformity may be attributed to the entry point of the air inlet. Consequently, a study on two similar designs that differ only in the location of the air inlet, as illustrated in Figure 12, was conducted. The numerical results are presented in Figure 11.
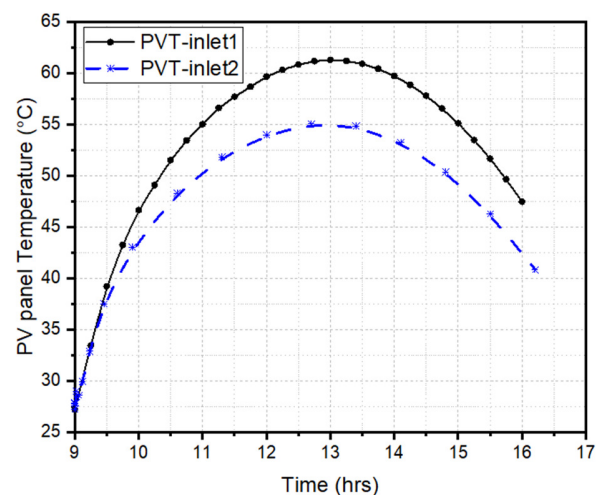

Fig. 11.   Progression of the temperature of the PV panel for the two air inlet scenarios.

A 3D study of the air distribution in the PVT was conducted for the two proposed scenarios of air entry into the collector. The results presented in Figure 12 disclosed that the

air velocity within the channels was more uniform in the PV/T system with Inlet-2 compared to the PV/T system with Inlet-1. This can be attributed to the prominent role played by the new design of the air inlet, where the air circulation and re-circulation were facilitated before reaching the air ducts. Thus, a gradual achievement of better air uniformity and consistency was observed as the air reached the channels. Conversely, in the first model, turbulence was evident at the entrance of the channels, leading to the presence of blind zones with weak air velocities resulting from the air re-circulation.
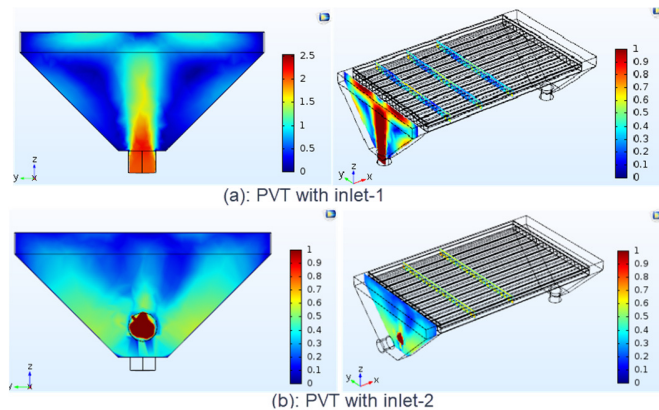

Fig. 12.   3D air flow distribution for the two air inlet scenarios of the PV/T.

E. Electrical and Thermal Performance Progression of the Proposed Designs

The effect of PV/T geometry was demonstrated by plotting the thermal efficiency and electrical efficiency versus the PV/T designs.
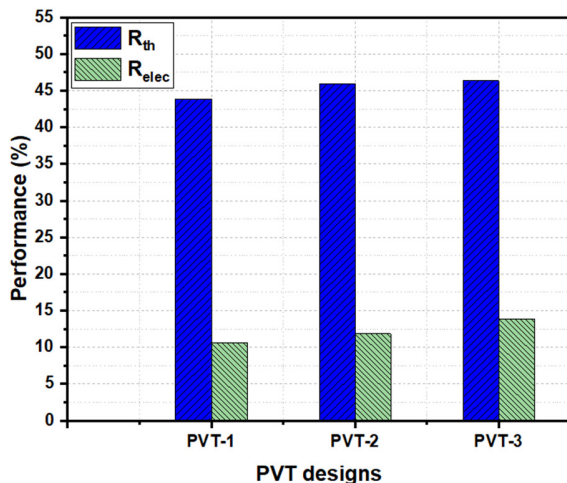

Fig. 13.   Evolution of the PVT performances versus their designs.

From the presented results in Figure 13, it can be observed that the PV/T design has a direct effect on its performance. Therefore, thermal and electrical efficiency increased from one design (PVT-1) to another (PVT-3). The enhancement of thermal performance is attributed to the influence of the design

of the air ducts channel. In Figure 13, it should be noted that the maximum average thermal efficiency of 46.35 % is obtained for PVT-3 and the minimum average thermal efficiency of 43.87 % for PVT-1. Similarly, the best electrical performance is 13.91% and is acquired with PVT-3, while the minimum electrical performance is 10.57% and is obtained by PVT-1.

IV.   CONCLUSION

The significance of his article resides in the pioneering design of a PV/T air collector, which serves as a central focus of the performed research. COMSOL Multiphysics was deployed to conduct a detailed numerical simulation and study how the air duct design and inlet position affect the electrical and thermal performance in the proposed PV/T designs. This study meticulously examined the relationship between the air duct designs and outlet temperature. The acquired numerical results clearly show that PVT-3 outperforms PVT-1 and PVT-2, exhibiting improved electrical and thermal performances. In particular, the prototype PVT-1, with square tube air ducts, reached a peak PV panel temperature of 61.5°C, whereas PVT-3, equipped with fin-shaped air ducts, recorded a minimum temperature of 55 °C. The PV/T collector attained peak power outputs: 82 W for PVT-1, 95 W for PVT-2, and 120 W for PVT-3. Results confirm PVT-3's superior electrical performance, showcasing how increasing the contact area between the air and the PV panel significantly boosts the overall electrical output. This improvement directly stems from the impactful influence of the air channel design on PV/T temperature regulation, orchestrated through the cooling phenomenon. These results offer valuable insights for optimizing cooling efficiency and the operational dynamics of PV cells across different air duct configurations, extending beyond mere temperature variations. Results indicate that the PV/T with Inlet-2 achieved superior airflow uniformity compared to that with Inlet-1, attributed to the redesigned inlet reducing turbulence and enhancing air circulation. Future research on PV/T systems may focus on: (1) Enhancing performance with advanced materials and (2) boosting flexibility and grid stability via energy storage integration.

ABBREVIATIONS

PV/T	Photovoltaic-Thermal collector
PV	Photovoltaic panel
D_1	Air gap height (m)
D_2	Flow duct height (m)
λ	Thermal conductivity (W/m.K)
Cp	Specific heat capacity (J/kg.K)
t	Time (s)
Q_{cv}	Convective heat loss (W)
Q_{abs}	Heat source absorber (W)
Q_{rd}	Radiation heat loss (W)
R_{th}	Thermal efficiency (%)
R_{elec}	Electrical efficiency (%)
T	Temperature (°C)
U	Velocity field (m/s)
u	Air flow velocity in the x direction (m/s)
v	Air flow velocity in the y direction (m/s)
w	Air flow velocity in the z direction (m/s)
x, y	Space coordinates
w_s	Wind velocity (m/s)
θ	Kinematic viscosity (m²/s)

V_{int}	Inlet velocity (m/s)
μ	Fluid dynamic viscosity (kg/(m.s))
I	Moment of inertia (kg.m²)
F	Force (N)
g	Gravity field (m/s²)
S	Section (m²)
I_{pv}	Current at the solar cell output (A)
I_{ph}	Photocurrent (A)
I_s	Saturation current (A)
I_{rs}	Reverse saturation current at the reference (A)
I_{scn}	Nominal short-circuit current (A)
V_{oc}	Open circuit voltage (V)
A	Diode ideality factor
K	Boltzmann constant
V_{pv}	Terminal voltage (V)
R_{sh}	Shunt resistance (Ω)
R_s	Series resistance (Ω)
K_i	Temperature coefficient of short circuit current
T_{w0}	Operating temperature of the cell (K)
Ird	Solar radiation (W/m²)
$hc_{g\text{-}D1}$	Coefficient of convection heat transfer between glass and air gap (W/m² K)
$hc_{pv\text{-}D1}$	Coefficient of convection heat transfer between PV and air gap (W/m² K)
$hc_{pv\text{-}D2}$	Coefficient of convection heat transfer between PV and air tube coefficient (W/m² K)
h_r	Radiative heat transfer coefficient (W/m² K)
h_w	Coefficient of convection heat transfer between glass and ambient (W/m² K)
δ	Thikness (m)
ρ	Density (kg/m³)
α	Apsorption coeffecient
σ	Stefan-Boltzman constant
ε	Emissivity coeffecient
τ	Transmisivity coeffecient
g	Glass
out	Outlet
a	Ambient
int	Inlet

ACKNOWLEDGMENT

REFERENCES

[1] M. Fterich, H. Chouikhi, H. Bentaher, and A. Maalej, "Experimental parametric study of a mixed-mode forced convection solar dryer equipped with a PV/T air collector," *Solar Energy*, vol. 171, pp. 751–760, Sep. 2018, https://doi.org/10.1016/j.solener.2018.06.051.

[2] M. Fterich, H. Chouikhi, S. Ghorbel, H. Bentaher, S. Sandoval-Torres, and A. Maalej, "Numerical and Experimental Study of Solar Dryer Equipped with PV/T," *Tehnički Vjesnik*, vol. 29, no. 3, pp. 896–906, Apr. 2022, https://doi.org/10.17559/TV-20200926203404.

[3] J. L. Holechek, H. M. E. Geli, M. N. Sawalhah, and R. Valdez, "A Global Assessment: Can Renewable Energy Replace Fossil Fuels by 2050?," *Sustainability*, vol. 14, no. 8, Jan. 2022, Art. no. 4792, https://doi.org/10.3390/su14084792.

[4] D. J. Soeder, "Greenhouse gas sources and mitigation strategies from a geosciences perspective," *Advances in Geo-Energy Research*, vol. 5, no. 3, pp. 274–285, Sep. 2021, https://doi.org/10.46690/ager.2021.03.04.

[5] A. L. Cowie *et al.*, "Applying a science-based systems perspective to dispel misconceptions about climate effects of forest bioenergy," *GCB Bioenergy*, vol. 13, no. 8, pp. 1210–1231, 2021, https://doi.org/10.1111/gcbb.12844.

[6] L. Gustavsson, T. Nguyen, R. Sathre, and U. Y. A. Tettey, "Climate effects of forestry and substitution of concrete buildings and fossil energy," *Renewable and Sustainable Energy Reviews*, vol. 136, Feb. 2021, Art. no. 110435, https://doi.org/10.1016/j.rser.2020.110435.

[7] P. Saosee, B. Sajjakulnukit, and S. H. Gheewala, "Environmental externalities of wood pellets from fast-growing and para-rubber trees for sustainable energy production: A case in Thailand," *Energy Conversion and Management: X*, vol. 14, May 2022, Art. no. 100183, https://doi.org/10.1016/j.ecmx.2022.100183.

[8] T. Singh *et al.*, "Emerging technologies for the development of wood products towards extended carbon storage and CO2 capture," *Carbon Capture Science & Technology*, vol. 4, Sep. 2022, Art. no. 100057, https://doi.org/10.1016/j.ccst.2022.100057.

[9] M. M. Akrofi, "An analysis of energy diversification and transition trends in Africa," *International Journal of Energy and Water Resources*, vol. 5, no. 1, pp. 1–12, Mar. 2021, https://doi.org/10.1007/s42108-020-00101-5.

[10] M. Li, M. Ahmad, Z. Fareed, T. Hassan, and D. Kirikkaleli, "Role of trade openness, export diversification, and renewable electricity output in realizing carbon neutrality dream of China," *Journal of Environmental Management*, vol. 297, Nov. 2021, Art. no. 113419, https://doi.org/10.1016/j.jenvman.2021.113419.

[11] C. Magazzino, M. Mele, N. Schneider, and U. Shahzad, "Does export product diversification spur energy demand in the APEC region? Application of a new neural networks experiment and a Decision Tree model," *Energy and Buildings*, vol. 258, Mar. 2022, Art. no. 111820, https://doi.org/10.1016/j.enbuild.2021.111820.

[12] P. Siemiński, J. Hadyński, J. Lira, and A. Rosa, "Regional Diversification of Electricity Consumption in Rural Areas of Poland," *Energies*, vol. 14, no. 24, Jan. 2021, Art. no. 8532, https://doi.org/10.3390/en14248532.

[13] G. Ślusarz, B. Gołębiewska, M. Cierpiał-Wolan, J. Gołębiewski, D. Twaróg, and S. Wójcik, "Regional Diversification of Potential, Production and Efficiency of Use of Biogas and Biomass in Poland," *Energies*, vol. 14, no. 3, Jan. 2021, Art. no. 742, https://doi.org/10.3390/en14030742.

[14] M. T. Alkhayyat, Z. S. Mohammed, and A. J. Ali, "Performance improvement of stand-alone induction generator using distribution SSC for wind power application," *Bulletin of Electrical Engineering and Informatics*, vol. 11, no. 2, pp. 589–601, Apr. 2022, https://doi.org/10.11591/eei.v11i2.2730.

[15] Y.-H. Ha and S. S. Kumar, "Investigating decentralized renewable energy systems under different governance approaches in Nepal and Indonesia: How does governance fail?," *Energy Research & Social Science*, vol. 80, Oct. 2021, Art. no. 102214, https://doi.org/10.1016/j.erss.2021.102214.

[16] K. Kang, N. B. Klinghoffer, I. ElGhamrawy, and F. Berruti, "Thermochemical conversion of agroforestry biomass and solid waste using decentralized and mobile systems for renewable energy and products," *Renewable and Sustainable Energy Reviews*, vol. 149, Oct. 2021, Art. no. 111372, https://doi.org/10.1016/j.rser.2021.111372.

[17] M. Moner-Girona, G. Kakoulaki, G. Falchetta, D. J. Weiss, and N. Taylor, "Achieving universal electrification of rural healthcare facilities in sub-Saharan Africa with decentralized renewable energy technologies," *Joule*, vol. 5, no. 10, pp. 2687–2714, Oct. 2021, https://doi.org/10.1016/j.joule.2021.09.010.

[18] A. Q. Jakhrani, A. R. Jatoi, M. M. Jakhrani, A. N. Laghari, and S. A. Kamboh, "Appraisal of Climatic Conditions for Potential Solar Energy Applications in Nawabshah and Quetta Cities," *Engineering, Technology & Applied Science Research*, vol. 9, no. 1, pp. 3711–3714, Feb. 2019, https://doi.org/10.48084/etasr.2472.

[19] I. Zeghib and A. Chaker, "Efficiency of a Solar Hydronic Space Heating System under the Algerian Climate," *Engineering, Technology & Applied Science Research*, vol. 6, no. 6, pp. 1274–1279, Dec. 2016, https://doi.org/10.48084/etasr.875.

[20] M. N. Hanani, J. Sampe, J. Jaffar, and N. H. M. Yunus, "Development of a Hybrid Solar and Waste Heat Thermal Energy Harvesting System," *Engineering, Technology & Applied Science Research*, vol. 13, no. 3, pp. 10680–10684, Jun. 2023, https://doi.org/10.48084/etasr.5561.